Lab on a Chip

View Online
Dynamic Article Links

Cite this: *Lab Chip*, 2011, **11**, 1502

www.rsc.org/loc

PAPER

Dual-color fluorescence cross-correlation spectroscopy on a planar optofluidic chip†

A. Chen,[a] M. M. Eberle,[a] E. J. Lunt,[b] S. Liu,[a] K. Leake,[a] M. I. Rudenko,[a] A. R. Hawkins[b] and H. Schmidt*[a]

Received 12th September 2010, Accepted 28th January 2011
DOI: 10.1039/c0lc00401d

Fluorescence cross-correlation spectroscopy (FCCS) is a highly sensitive fluorescence technique with distinct advantages in many bioanalytical applications involving interaction and binding of multiple components. Due to the use of multiple beams, bulk optical FCCS setups require delicate and complex alignment procedures. We demonstrate the first implementation of dual-color FCCS on a planar, integrated optofluidic chip based on liquid-core waveguides that can guide liquid and light simultaneously. In this configuration, the excitation beams are delivered in predefined locations and automatically aligned within the excitation waveguides. We implement two canonical applications of FCCS in the optofluidic lab-on-chip environment: particle colocalization and binding/dissociation dynamics. Colocalization is demonstrated in the detection and discrimination of single-color and double-color fluorescently labeled nanobeads. FCCS in combination with fluorescence resonance energy transfer (FRET) is used to detect the denaturation process of double-stranded DNA at nanomolar concentration.

Introduction

Fluorescence correlation spectroscopy (FCS) includes several powerful techniques to study extremely low concentrations of biomolecules or bioparticles by measuring the fluctuation of the fluorescence intensity, which can arise from the diffusion of biomolecules in and out of an excitation volume or by the conformational fluctuation of biomolecules caused by chemical or photo-physical interactions.[1,2] In conventional FCS, the time-dependent autocorrelation of the fluctuations from a single fluorescence signal is analyzed to extract information about molecular concentration, kinetic coefficients, flow velocities, *etc.*[3] Fluorescence cross-correlation spectroscopy (FCCS) is an important extension of FCS, in which the cross-correlation between two different fluorescence signals at different colors is computed. As such, FCCS gives a quick yes or no answer to the concurrence of two spectrally distinct fluorophores. This approach is especially advantageous for monitoring molecular interactions or the dynamics of colocalization, providing extra capability of detecting multiple targets simultaneously with enhanced sensitivity.[4] Since the first experimental demonstration of dual-color FCCS,[5] numerous implementations and applications of FCCS techniques have been developed, ranging from enzymatic cleavage of oligonucleotides[6] to protein–protein interactions[7,8] and more recently, the detection of influenza virus.[9] More examples and details can be found in dedicated reviews.[4,10]

Generally, FCS and FCCS have been implemented using a confocal microscope which typically consists largely of bulk optical components. FCCS, in particular, requires substantial experimental effort to align multiple beam paths on top of (dual-color FCCS) or relative to each other (dual-focus FCCS). Unlike single molecule detection, neither FCS nor FCCS requires surface immobilization; thus correlation spectroscopy is very attractive for implementation in a lab-on-chip setting involving directed flow or diffusive motion in micro-scale channels. Indeed, both FCS and FCCS have been successfully demonstrated in semi-integrated environments, including DNA fragment sizing in nanofluidic channels,[11] microfluidic cell culture systems,[12] and on-chip virus detection.[13] However, problems with alignment of multiple laser foci within the microfluidic channels have limited such approaches.[13] Therefore, a more complete approach to integration in which optical beams are delivered *via* integrated waveguides is highly desirable. We have previously demonstrated FCS detection and analysis of single molecules and single bioparticles in optofluidic chips based on anti-resonant reflecting optical waveguides (ARROW).[14,15] FCCS stands to benefit even more from such integrated approaches since the alignment of multiple optical beams and the definition of multiple excitation volumes are easily accomplished using lithographically defined waveguide structures and off-the-shelf fiber optics. Here, we present the first implementation of two-color FCCS detection on a planar optofluidic platform and demonstrate two types of

[a]*School of Engineering, University of California Santa Cruz, MS: SOE-2, 1156 High Street, Santa Cruz, CA, 95064, USA. E-mail: hschmidt@soe.ucsc.edu; Fax: +1-831-459-4829; Tel: +1-831-459-1482*
[b]*ECE Department, Brigham Young University, Provo, UT, 84602, USA*
† Electronic supplementary information (ESI) available: Additional experimental parameters and FCS analysis results are presented. See DOI: 10.1039/c0lc00401d

applications for which FCCS is superior to conventional single-beam FCS. First, we use two-color FCCS to detect colocalization of fluorescent dyes on nanobeads and discriminate between singly labeled and doubly labeled nanobeads. Secondly, we combine fluorescence resonance energy transfer (FRET) and FCCS techniques using a single excitation laser to detect temperature-induced dissociation of double-stranded DNA at nanomolar concentration.

Experimental

The planar FCCS platform and ARROW fabrication

A liquid-core ARROW forms the basis of our planar optofluidic chip. The geometry of a typical ARROW consists of a hollow core filled with low-refractive index liquids surrounded by one or more cladding layers of higher refractive index. If the cladding layer thicknesses fulfill the antiresonant condition, similar to an antiresonant Fabry–Pérot cavity, most of the energy (optical mode) will remain within the waveguide core.[16,17] A complete optofluidic platform is created by interfacing these liquid-core waveguide channels with solid-core ARROW waveguides. Light from the chip edges and liquid from μL fluidic reservoirs are delivered independently to a central liquid-core waveguide section.[18]

A schematic of the FCCS optofluidic chip is shown in Fig. 1(a) with solid-core waveguides denoted as white blocks and liquid-core waveguides denoted as blue blocks. 488 nm and 633 nm lasers are combined by a dichroic mirror then coupled into a single mode fiber. The output of the fiber is coupled into the solid-core of the ARROW, thus guaranteeing the crucial overlap of the excitation beams at the excitation location. The excitation volume itself is lithographically defined by the intersection of the solid-core input waveguide with the liquid-core waveguide. The shape of this excitation volume is approximated very well by three Gaussian profiles[19] (half widths $w_x = 4.5$ μm, $w_y = 1.6$ μm, $w_z = 4.5$ μm), resulting in a total excitation volume of $V = 4/3\pi w_x w_y w_z \approx 135$ fL. Fluorescently labeled biomolecules and bioparticles are injected into one reservoir and flow to the other reservoir under a positive or negative pressure differential. The planar waveguide geometry enables detection of fluorescence signals from labeled particles through separate paths (see Fig. 1a). Here, two distinct wavelengths are recorded simultaneously by inserting bandpass filters in front of single photon avalanche photodiodes (SPADs). These two channel signals, $F_1(t)$ and $F_2(t)$ are processed by a Time Harp 200 (Picoquant) PCI-board with a PRT 400 router in a time-tagged time resolved mode (for additional details see ESI†). The correlation function $G_{ij}(\tau)$ ($i = j$: autocorrelation, $i \neq j$: cross-correlation) is defined as:[6]

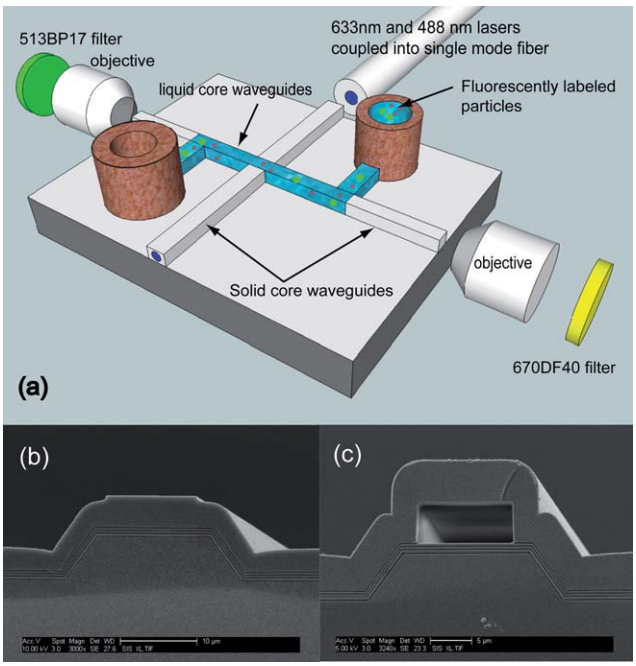

Fig. 1 (a) Planar FCCS detection platform. A 488 nm argon laser and a 633 nm He–Ne laser are combined with a dichroic mirror and coupled into a single-mode fiber by a fiber coupler, and then coupled in a solid-core ARROW, which intersects a liquid-core ARROW. Fluorescently labeled particles are injected into one reservoir and flow through the liquid-core ARROW. Different colors of fluorescence are collected by SPADs after filtering by the bandpass filters. Bandpass filters (center wavelength 513 (670) nm; width 17 (40) nm) are mounted in the beam paths of liquid-core direction. The SEM images show the cross-sectional images of a solid-core (b) and a liquid-core (c) ARROW, respectively.

$$G_{ij}(\tau) = \frac{\langle \delta F_i(t) \delta F_j(t+\tau) \rangle}{\langle F_i(t) \rangle \langle F_j(t) \rangle} \quad (1)$$

where $\langle F_i(t) \rangle$ is the time-averaged fluorescence in color channel i ($i = 1$ or 2), $\delta F_i(t) = F_i(t) - \langle F_i(t) \rangle$ is the fluorescence fluctuation and τ is the lag time. Besides the above cross-correlation function, we adapt the previously published ARROW FCS model to fit the data collected from the optical excitation/detection volume obtained from waveguide mode simulations.[15,19]

The fabrication of ARROWs is based on photolithography, wet etching, and plasma enhanced chemical vapor deposition (PECVD). For the samples used here, a single overcoat silicon dioxide layer was deposited on top of alternating layers of silicon dioxide and silicon nitride that provide optical waveguiding as previously described.[18,20,21] Fluidic reservoirs of ~10 μL volume are attached to the open ends of the hollow-core waveguide using epoxy (see Fig. 1a).

Fluorescence cross-correlation spectroscopy (FCCS) from singly and doubly labeled nanobeads

In order to demonstrate the power of cross-correlation spectroscopy on an optofluidic platform, colocalization of fluorescent dyes on polystyrene nanobeads was investigated. First, a mixture of 100 nm Yellow-green beads (excitation/emission[nm]: 505/515) and 40 nm Dark-red beads (excitation/emission [nm]: 660/680) was introduced into one of the fluid reservoirs (the other was kept empty). Driven by the pressure difference, nanobeads flowed across the excitation region, the fluorescence bursts were guided along the liquid core and collected at both chip ends, as indicated in Fig. 1(a). Both color channels were recorded simultaneously at 100 ns time resolution synchronized by a function generator. The fluorescence signal from the two bead types was integrated over 5 ms bins, as shown in the inset of Fig. 2(a). The autocorrelation and cross-correlation functions between the two color channels are calculated based on eqn (1).

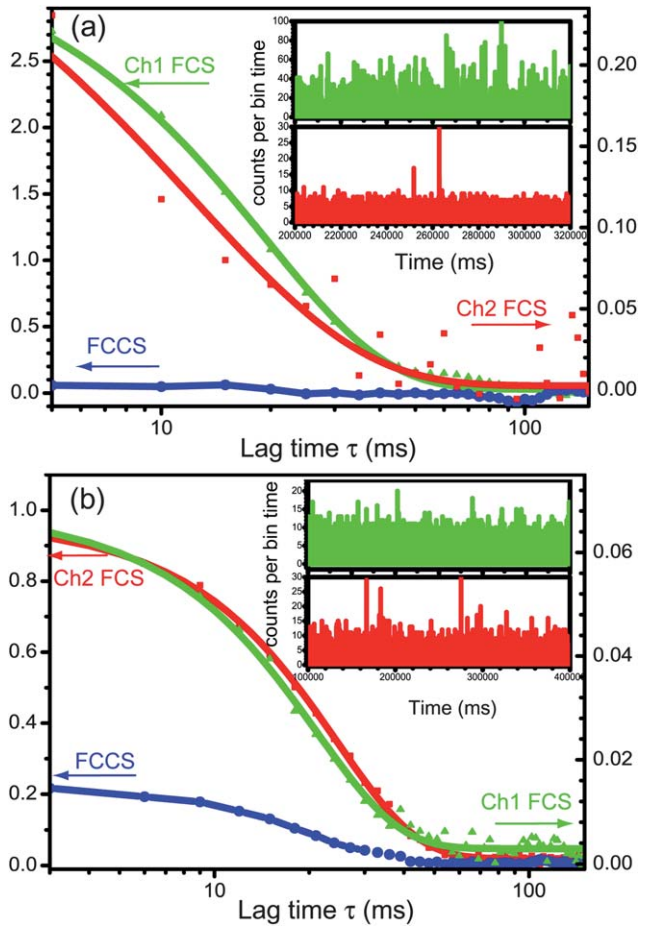

Fig. 2 FCS from (a) singly labeled nanobeads: 100 nm Yellow-green beads (green curve with triangle symbols, absorption/emission 505/515 after 513BP17 filter) and 40 nm Dark-red beads (red curve with square symbols, absorption/emission 660/680 after 670DF40 filter), both at 5 ms bin time. (b) FCS from doubly labeled 100 nm TetraSpeck beads at 3 ms bin time with same filter set. In both (a) and (b), FCCS data are denoted by blue circles and insets are the time histograms from individual bursts. Doubly labeled nanobeads can be clearly identified by a non-zero FCCS.

The fitted autocorrelation function indicates that the flow velocities are 69.3 μm s^{-1} for 100 nm yellow green and 70.7 μm s^{-1} for 40 nm dark red beads, respectively, indicating that particle motion is dominated by the solvent flow. This is reasonable since the mixture of both beads is mostly driven by liquid flow (pressure driven) across the excitation volume. However, as shown in the blue curve in Fig. 2(a), the fluorescence cross-correlation between 100 nm and 40 nm beads is nearly zero, which suggests that over large numbers of event statistics, the chance of seeing simultaneous fluorescence from both beads is close to zero since they are from different targets.

The experiment was repeated with 100 nm TetraSpeck beads, which are labeled with multi-color (excitation/emission [nm]: 360/430, 505/515, 560/580, 660/680) dyes on the same bead. The autocorrelation and cross-correlation signals between the two color (505/515 and 660/680) channels are displayed in Fig. 2b. Here, the difference in autocorrelation amplitudes is attributed to the different quantum efficiencies of different color dyes on beads and the different spectral widths of bandpass filters. In contrast to Fig. 2(a), we now find a strong cross-correlation between two different emission channels (blue circles in Fig. 2b) which is expected since these two fluorescence colors now originate from the same target bead.

Application: detecting DNA dissociation *via* FCCS

A second classic area in which FCCS is superior to conventional fluorescence spectroscopy is the detection of dynamic molecular processes, in particular binding and dissociation events. Here, we demonstrate this capability using a biologically relevant application. FCCS on double-stranded DNA is used to identify DNA dissociation with much higher sensitivity than single color FCS. To this end, oligonucleotide sequences of 5′-TGC AGC GAG TTC AGC/3Cy3Sp/-3′ and 5′-/5Cy5/AT GCT GAA CTC GCT GCA-3′ were designed (Integrated DNA Technologies; two extra bases were added on purpose to prevent steric clash between the dyes after annealing). In this configuration, Cy3 and Cy5 fluorescent dyes are located at the same end after annealing, allowing us to combine FCCS with fluorescence resonance energy transfer (FRET). FRET is another popular technique for molecular dynamics studies and is based on energy transfer of an optically excited donor molecule (in this case Cy3) to a closely spaced acceptor molecule (Cy5) *via* dipole–dipole coupling.[1] However, FRET typically requires surface immobilization, is limited to detecting distances in the 1–10 nm range, and is more susceptible to photobleaching than FCCS which relies on statistical analysis of fluorescence bursts on much shorter time scales (from a few μs to a few ms). Here, we use FRET to generate a two-color cross-correlation signal from a single excitation source.

For the experiment, double-stranded DNAs (or FRET pairs) were prepared by mixing donor and acceptor oligonucleotides at equal concentrations (typically 20 μM) and annealing at ~55 °C for 2 minutes and then slowly cooling to room temperature for about one hour. The stock oligonucleotide solution was stored in a freezer and diluted to a low concentration (in TE buffer: 10 mM Tris–HCl, pH 8.0 and 1 mM EDTA) right before use. To reduce DNA sticking to the walls of the microfluidic channel, bovine serum albumin (BSA) was first introduced to the channel followed by flushing with TE buffer.

Since we realize FCCS by FRET, it is necessary to examine FRET efficiency and see how well energy is transferred between the donor and the acceptor. For this set of experiments, a single excitation laser (λ = 532 nm) was fiber-coupled to a solid-core ARROW. Cy3 and Cy5 labeled double-stranded DNA molecules (FRET pairs) were injected into one reservoir and flowed through the liquid-core ARROW. Once the oligonucleotides passed through the intersection and were excited by the laser, the fluorescence emissions from the donor and the acceptor were guided through the liquid-core ARROW and collected at both chip ends. The donor and acceptor fluorescence were filtered with 585BP40 and 670DF40 filters, respectively. We first determined the energy transfer efficiency based on:[22]

$$E = \left(1 + \gamma \frac{I_D}{I_A}\right)^{-1} \quad (2)$$

where I_i (i = D or A) is the donor or acceptor fluorescence intensity. γ is a correction factor, which accounts for the differences in quantum yield and detection efficiency between the donor and the acceptor. γ is calculated as the ratio of intensity

change in the acceptor and in the donor by photobleaching the acceptor ($\gamma = \Delta I_A/\Delta I_D$). In order to extract γ, a separate photobleaching beam (a 15 mW 565 nm green laser from an optical parameter oscillator) was launched along the liquid core to photobleach all acceptor molecules along the entire 4 mm long fluidic channel. This approach reveals another advantage of the planar waveguide integration since application of the bleaching beam to the entire channel and not just the excitation volume prevents errors due to diffusion of new acceptor dye into the small excitation volume. After background subtraction and γ correction, we obtained a FRET efficiency of ~91% in good agreement with the expectations from the oligonucleotide structure. In order to combine FRET with FCCS, we reduced the concentration down to ~1.2 nM to effectively resolve individual fluorescence bursts as the DNA molecules travel across the excitation volume. Two different color emissions from both the donor and the acceptor were recorded after the filters and analyzed like the nanobeads to calculate the correlation functions.

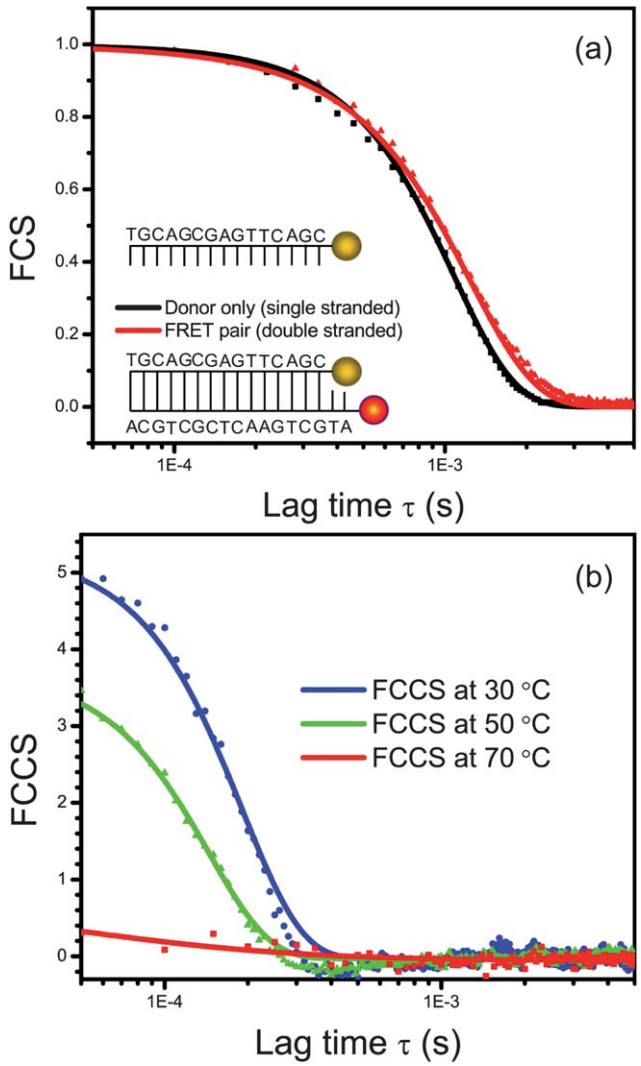

Fig. 3 (a) Normalized donor emission autocorrelation from single-stranded (black curve with square symbols) and double-stranded DNA (red curve with triangle symbols). FCS curves show a small shift due to differing diffusion coefficients. (b) Denaturation of double-stranded DNA detected *via* temperature-dependent FCCS. Spatial separation of donor and acceptor dye leads to loss of cross-correlation at high temperatures.

The advantages of FCCS over FCS are illustrated in Fig. 3. Fig. 3(a) shows the normalized fluorescence autocorrelations from Cy3 labeled single-stranded oligonucleotides (black curve with square symbols) and double-stranded DNA (red curve with triangle symbols). Since the size of the single-stranded and double-stranded DNA was very similar, the difference in their diffusion coefficients was also small. In other words, if double-stranded DNA was dissociated into two single-stranded oligonucleotides, it can be challenging to detect them based on single color FCS as shown in Fig. 3(a), especially in cases of poor signal-to-noise ratio. Next, we collected both the donor and acceptor emissions from double-stranded DNA (FRET pairs). At the same time, the ARROW integrated chip was heated with a thermoelectric cooler module with temperature feedback regulation. To reduce heating induced liquid evaporation from the reservoir, 2 μL of mineral oil was applied on top of the 8 μL fluid's surface. Fig. 3(b) shows the FCCS curve correlated from both the donor channel (Cy3 emission, after 585BP40 filter) and acceptor channel (Cy5 emission, after 670DF40 filter) as the temperature was increased. Since the annealing temperature of these oligonucleotides was near 55 °C, as the temperature was increased, double-stranded DNA had dissociated into single-stranded oligonucleotides and both FRET and FCCS decreased. Thus, the transition from double-stranded DNA to single-stranded DNA was revealed very clearly using FCCS, providing a much more obvious distinction between double to single-stranded nucleotides than the relatively small shift in the single-color FCS signal of Fig. 3(a). We note that the FCCS value may be somewhat increased due to cross-talk between the donor and acceptor from FRET. Nevertheless, it is an excellent indicator of binding and dissociation events and the cross-talk complication could be avoided by labeling the DNA strands at opposite ends and using dual color FCCS.[6]

Conclusions

In summary, we have demonstrated fluorescence cross-correlation spectroscopy on a planar optofluidic chip using integrated optical waveguides to achieve a performance comparable to traditional (confocal) microscopy approaches. In addition to adding the mere convenience of a compact platform, the combination of solid and liquid-core waveguides provides specific advantages for implementation of cross-correlation modalities: straightforward integration and alignment of multiple-color laser sources for multi-color spectroscopy; spatially separated detection paths for multiple signal wavelengths; and simple incorporation of additional control beams (*e.g.* for acceptor photobleaching or particle guiding[23]). These unique features of the optofluidic approach were used to demonstrate two main application areas of cross-correlation spectroscopy. Dual-color FCCS was used for detection and discrimination of nanobeads with separate or colocalized fluorescent dyes. In addition, single-beam FCCS/FRET detection was applied to observe denaturing of the DNA at low concentration and much more clearly compared to FCS. These representative examples illustrate that the planar waveguide geometry

is well suited for demanding applications that involve multiple optical beams for signal generation, collection, and control. In the future, multi-color spectroscopy techniques such as FRET and FCCS can be further improved by incorporating spectral filter functions,[17,24,25] pointing the way towards self-contained optofluidic labs on a chip.

Acknowledgements

We thank P. Measor for useful discussions, and D. N. Ermolenko for providing DNA sequences. This work was supported by the NIH/NIBIB (grant R01EB006097), NSF (grants ECS-0528730 and ECS-0528714), and the W. M. Keck Center for Nanoscale Optofluidics at UCSC.

References

1 J. R. Lakowicz, *Principles of Fluorescence Spectroscopy*, Springer, 3rd edn, 2006.
2 O. Krichevsky and G. Bonnet, *Rep. Prog. Phys.*, 1997, **65**, 251.
3 C. Zander, J. Enderlein and R. A. Keller, *Single-Molecule Detection in Solution Methods and Applications*, Wiley-VCH, 1st edn, 2002.
4 K. Bacia, S. A. Kim and P. Schwille, *Nat. Methods*, 2006, **3**, 83–89.
5 P. Schwille, F. Meyer-Almes and R. Rigler, *Biophys. J.*, 1997, **72**, 1878–1886.
6 U. Kettling, A. Koltermann, P. Schwille and M. Eigen, *Proc. Natl. Acad. Sci. U. S. A.*, 1998, **95**, 1416–1420.
7 N. Baudendistel, G. Müller, W. Waldeck, P. Angel and J. Langowski, *ChemPhysChem*, 2005, **6**, 984–990.
8 E. Zamir, P. H. M. Lommerse, A. Kinkhabwala, H. E. Grecco and P. I. H. Bastiaens, *Nat. Methods*, 2010, **7**, 295–298.
9 S. Huet, S. V. Avilov, L. Ferbitz, N. Daigle, S. Cusack and J. Ellenberg, *J. Virol.*, 2010, **84**, 1254–1264.
10 S. A. Kim, K. G. Heinze, M. N. Waxham and P. Schwille, *Proc. Natl. Acad. Sci. U. S. A.*, 2004, **101**, 105–110.
11 M. Foquet, J. Korlach, W. Zipfel, W. W. Webb and H. G. Craighead, *Anal. Chem.*, 2002, **74**, 1415–1422.
12 C. Zhang, S. Chia, S. Ong, S. Zhang, Y. Toh, D. van Noort and H. Yu, *Biomaterials*, 2009, **30**, 3847–3853.
13 Y. Zhang, J. T. Bahns, Q. Jin, R. Divan and L. Chen, *Anal. Biochem.*, 2006, **356**, 161–170.
14 D. Yin, E. J. Lunt, M. I. Rudenko, D. W. Deamer, A. R. Hawkins and H. Schmidt, *Lab Chip*, 2007, **7**, 1171–1175.
15 M. I. Rudenko, S. Kühn, E. J. Lunt, D. W. Deamer, A. R. Hawkins and H. Schmidt, *Biosens. Bioelectron.*, 2009, **24**, 3258–3263.
16 M. A. Duguay, Y. Kokubun, T. L. Koch and L. Pfeiffer, *Appl. Phys. Lett.*, 1986, **49**, 13.
17 H. Schmidt, D. Yin, J. Barber and A. R. Hawkins, *IEEE J. Sel. Top. Quantum Electron.*, 2005, **11**, 519–527.
18 H. Schmidt and A. R. Hawkins, *Microfluid. Nanofluid.*, 2007, **4**, 3–16.
19 D. Yin, E. J. Lunt, A. Barman, A. R. Hawkins and H. Schmidt, *Opt. Express*, 2007, **15**, 7290.
20 E. J. Lunt, P. Measor, B. S. Phillips, S. Kühn, H. Schmidt and A. R. Hawkins, *Opt. Express*, 2008, **16**, 20981–20986.
21 A. Hawkins and H. Schmidt, *Microfluid. Nanofluid.*, 2008, **4**, 17–32.
22 R. Roy, S. Hohng and T. Ha, *Nat. Methods*, 2008, **5**, 507–516.
23 P. Measor, S. Kühn, E. J. Lunt, B. S. Phillips, A. R. Hawkins and H. Schmidt, *Opt. Express*, 2009, **17**, 24342–24348.
24 B. S. Phillips, P. Measor, Y. Zhao, H. Schmidt and A. R. Hawkins, *Opt. Express*, 2010, **18**, 4790–4795.
25 P. Measor, B. S. Phillips, A. Chen, A. R. Hawkins and H. Schmidt, *Lab Chip*, 2011, **11**, 899–904.

